NIH Public Access
Author Manuscript
Anal Chem. Author manuscript; available in PMC 2014 April 02.

Published in final edited form as:
Anal Chem. 2013 April 2; 85(7): 3621–3628. doi:10.1021/ac303441n.

Scanning ion conductance microscopy measurement of paracellular channel conductance in tight junctions

Chiao-Chen Chen[1], **Yi Zhou**[1], **Celeste A. Morris**[1], **Jianghui Hou**[2,3,*], and **Lane A. Baker**[1,*]

[1]Department of Chemistry, Indiana University, 800 E. Kirkwood Avenue, Bloomington, Indiana 47405

[2]Renal Division, Washington University Medical School, 660 South Euclid Avenue, St. Louis, Missouri 63110.

[3]Center for Investigation of Membrane Excitability Diseases, Washington University Medical School, 660 South Euclid Avenue, St Louis, Missouri 63110.

Abstract

Elucidation of epithelial transport across transcellular or paracellular pathways promises to advance the present understanding of ion transport and enables regulation of cell junctions critical to the cell and molecular biology of the epithelium. Here we demonstrate a new instrumental technique potentiometric scanning ion conductance microscopy (P-SICM) that utilizes a nanoscale pipette to differentiate paracellular and transcellular transport processes at high spatial resolution. The technique is validated for well-defined polymer membranes and then employed to study wild type and claudin-deficient mutants of Madin-Darby Canine Kidney strain II (MDCKII) cells. Paracellular permeabilities conferred by claudin-2 are captured by P-SICM which demonstrates the utility to monitor apparent conductance at subcellular levels.

INTRODUCTION

Transport processes across the epithelium can take place through energy-dependent transcellular pathways or passive paracellular pathways, independently or synergistically.[1-3] Integral to paracellular transport through cell-cell junctions are organelles known as tight junctions (TJs) which form barriers to transport across the tissue interface.[4] Claudin proteins have been shown to confer ion selectivity to tight junctions (as demonstrated through resistance and permeability measurements) to form paracellular channels. For instance, permeability studies of paracellular channels have indicated the presence of 4-7 Å (in diameter) channels with chemically selective transport properties analogous to membrane-spanning ion channels.[5-7] Imbalances in paracellular transport of water and ions are often observed with claudin mutations and are further implicated in a number of pathological phenotypes with consequences that range from deafness to death.[8-15] The wide-ranging phenotypes caused by claudin dysfunction have raised a series of fundamental questions related to the cell and molecular biology of tight junctions. To study epithelial transport, recording techniques that make use of Ussing chambers to measure paracellular channel

[*]**Corresponding author:** Lane A. Baker Department of Chemistry Indiana University 800 E. Kirkwood Avenue Bloomington, Indiana 47405 (812) 856 1873; (812) 856 8300 (fax); lanbaker@indiana.edu; Jianghui Hou Department of Internal Medicine – Renal Division Division of Biological and Biochemical Sciences Washington University School of Medicine 660 South Euclid Avenue, Campus Box 8126 St. Louis, MO 63110 (314) 362 5685; (314) 362 8237 (fax); jhou@dom.wustl.edu.

SUPPORTING INFORMATION Supporting information is available on the Analytical Chemistry website http://pubs.acs.org/journal/ancham. Recombinant DNA experiments were approved by the institutional biological safety committee for the use of transgenic engineering.

NIH-PA Author Manuscript
NIH-PA Author Manuscript
NIH-PA Author Manuscript

NIH-PA Author Manuscript

NIH-PA Author Manuscript

NIH-PA Author Manuscript

conductance across polarized epithelium have been developed.[16-20] While informative, these previous recordings, reflect the aggregate response of thousands, or even millions of channel permeabilities, with current density as high as $\mu A/cm^2$. Clearly, such measurements lack subcellular spatial resolution. Unlike transcellular channels that can be recorded with patch clamp techniques, paracellular channels are located across the cell-cell boundary, which prevents formation of the necessary gigaohm seal between pipette and membrane. Potential scanning techniques for discrimination between trans- and paracellular pathways were first introduced by Frömter in 1972, where potential distributions above the surface of a single-layered epithelium were examined.[21] More quantitative conductance measurements with potential scanning techniques have been described, notably by the groups of Fromm[22-30] and Cereijido.[31-33] These measurements have been integral to understanding the role of junctional proteins in paracellular transport[25-26] and have been applied to cell monolayers[22, 24, 31-34] and even epithelial tissue.[23, 35] This powerful technique, however, has only been mastered by a few groups.[22, 31] Inspired by these pioneering works, we have utilized advanced control of the position of pipette electrodes afforded by scanning ion conductance microscopy (SICM) to enable subcellular resolution and more intuitively quantitative measurements of local conductances.

Scanning ion conductance microscopy makes use of a scanned pipette probe and was first described by Hansma et al in 1989.[36] A key feature of SICM is the ability to precisely control position of a pipette by monitoring changes in ion current that develop when the pipette is close to a surface (Figure 1a). We have previously demonstrated measurement of ion conductance at nanoporous polyimide membranes, a simplified biophysical model for tight junctions in an epithelial monolayer.[37-40] Here, through a dual-barrel probe design, SICM is extended to measure variations in potential generated over membranes and cell monolayers, which we term potentiometric SICM (P-SICM, Figure 1). An electrode in one barrel of the pipette monitors ion current to maintain a constant probe-surface distance (D_{ps}). Samples are mounted in a conductivity cell and a potential difference is applied across a sample (V_T). An electrode in the second barrel of the pipette then measures changes in apparent conductance, induced by V_T, over conductive pathways of the sample.

The optimized P-SICM design allows measurement of membranes with moderate permeabilities and can be applied to measurement of biological samples, namely polarized Madin-Darby Canine Kidney strain II (MDCKII) cells. High-resolution images of the apical membrane of MDCKII cells were first generated, followed by measurement of local conductances for paracellular and transcellular pathways. We then demonstrate the utility of this technique to monitor mutation-induced changes in paracellular channel properties of MDCKII cells. Charge and size selectivity of paracellular permeability conferred by claudin-2 is captured by P-SICM.

EXPERIMENTAL SECTION

SICM Instrumentation for Potential-based Measurements

In experiments described here, a modified ScanIC scanning ion conductance microscope (ionscope, London, U.K.) was utilized, as shown in Figure 1. A specimen of interest was mounted between two chambers of a conductivity cell, and a theta pipette was employed as a scanning probe. One barrel of the pipette, the pipette electrode (PE), served to position the probe and was biased at 100-150 mV (vs. reference electrode (RE)); the second barrel of the theta pipette was connected to a differential amplifier (a high impedance operational amplifier which is considered to have zero current flow), and is described as the potential electrode (UE), where localized changes in electrical potential (as opposed to ion current) with respect to the RE were examined. A Pt counter electrode (CE) located in the upper chamber was connected to a CE driver, which is enclosed in the electrode control unit

NIH-PA Author Manuscript

NIH-PA Author Manuscript

NIH-PA Author Manuscript

shown in Figure 1a. The CE was utilized to drive the majority of transmembrane current to prevent fluctuations in the potential of the RE.[40] Potential variations in the vicinity of a permeable membrane were induced by the application of transmembrane potentials (V_T) at the working electrode (WE). Explicitly, V_T represents the potential difference between the WE and the RE, which includes potential drops (1) across the monolayer, (2) between the monolayer and the WE, and (3) between the monolayer and the RE. However, as a result of the high resistance of epithelial monolayers (compared with the low resistance of buffer solutions) used here, >99% of V_T is localized across the epithelial monolayer. Consequently, V_T is a reasonable approximation of the potential drop across the epithelial monolayer, as illustrated in Figure 1b.

Potential-based measurement allows assessment of the apparent transepithelial/transmembrane conductance (G) with the following equation:[22, 31]

$$G=\left(\frac{E}{\rho \cdot V^e}\right)$$

in which E represents the electric field (potential gradient) measured with the UE, ρ indicates the specific resistance of the bath electrolyte and V^e is the potential range swept to induce the potential gradient recorded. The apparent transepithelial conductance (G, unit: S/cm^2) is the reciprocal of the transepithelial resistance (TER, unit: Ω·cm^2), an index commonly utilized in electrophysiology to evaluate the integrity and permeability of epithelial monolayers.

Cell Culture

Polarized Madin-Darby Canine Kidney (MDCK) strain II cell lines, wild-type (MDCKII-WT) and a claudin-2 depleted mutant (MDCKII-C2)[18] were routinely maintained in T-flasks at 37°C in a humidified air atmosphere (97% humidity) with 5% CO_2. The growth medium utilized was Dulbecco's modified Eagle's medium (DMEM, D6429, Sigma-Aldrich, MO) supplemented with 10% (v/v) fetal bovine serum (F4135, Sigma-Aldrich, MO), 100 U/mL penicillin and 100 μg/mL streptomycin (P0781, Sigma-Aldrich, MO). Additionally, 10 μg/mL of puromycin dihydrochloride was added for MDCKII-C2 cells, where endogenous expression of claudin-2 was knocked down by siRNA co-expressed with a puromycin resistance gene.[18]

When grown to confluence, cells were harvested with trypsin-EDTA (T4174, Sigma-Aldrich, MO) and plated with high density (10^6 cells/cm^2) on a collagen-coated membrane insert. The collagen-coated membrane was prepared by addition of 150 μg/cm^2 of collagen (C8919, Sigma-Aldrich, MO) onto a transparent porous PET membrane (pore diameter 0.4 μm, pore density 2×10^6 pores/cm^2, BD Falcon™, NJ). Cell monolayers cultured on membrane supports were maintained at 37°C in a humidified air-5% CO_2 atmosphere for 8-9 days to achieve confluence that displayed steady-state transepithelial resistance (TER). Immediately prior to experiments performed at room temperature in ambient atmosphere, the culture medium was changed to modified DMEM without $NaHCO_3$ (D7777, Sigma-Aldrich, MO) supplemented with 10% (v/v) fetal bovine serum, 44 mM NaCl and 25 mM HEPES (H0887, Sigma-Aldrich, MO).

Ion Replacement Experiment

Claudin-2 has been reported to contribute to paracellular permeability of small cations and water molecules for "leaky epithelia", such as the small intestine and kidney proximal

NIH-PA Author Manuscript

NIH-PA Author Manuscript

NIH-PA Author Manuscript

tubules.[41-42] Herein, charge selectivity of claudin-2 based paracelluar pathways was interrogated by P-SICM to further demonstrate the utility of this method.

Localized conductance measurements for control experiments were performed on MDCKII-WT and MDCKII-C2 monolayers with both apical and basolateral sides of container inserts filled with buffer A (137 mM NaCl, 5 mM KCl, 1 mM $MgCl_2$, 2 mM $CaCl_2$, 8 mM Mannitol and 10 mM HEPES). To examine cation selectivity, conductance measurements were repeated with buffer A on the basolateral side of culture inserts replaced with buffer B (5 mM NaCl, 132 mM NMDG-Cl, 5 mM KCl, 1 mM $MgCl_2$, 2 mM $CaCl_2$, 8 mM Mannitol and 10 mM HEPES). In buffer B, Na^+ was reduced to 5 mM by isomolar replacement of 132 mM NaCl with N-methyl-D-glucamine chloride (NMDGPCl). The same procedure was applied to examine anion selectivity, except buffer A on the basolateral side was replaced with buffer C (137 mM NaGlu, 5 mM KCl, 1 mM MgGlu, 2 mM CaGlu, 8 mM Mannitol and 10 mM HEPES), in which Cl^- concentration was reduced to 5 mM via replacement with gluconate (Glu^-). Both $NMDG^+$ and Glu^- are considered as impermeable ions to both trans and paracellular pathways.[43-44]

Statistical Analysis

Values of local conductance (G) are reported as the mean ± SD of measurements performed on three monolayers for each condition and are representative of at least two independent experiments, unless stated otherwise. Shapiro-Wilk test with an alpha level of 0.05 was utilized to assess the normality. Differences between groups with normal distribution were assessed with independent two-sample t-test while the Mann-Whitney test, a non-parametric alternative of independent two-sample t-test, was applied for data sets not from normally distributed populations. The alpha level for independent two-sample t-test and the Mann-Whitney test was 0.05 and the resultant $p\text{-}value < 0.05$ was considered statistically significant. Significance levels are denoted as * $p < 0.05$, ** $p < 0.01$, *** $p < 0.001$; n = number of observations.

RESULTS

Potentiometric scanning ion conductance microscopy (P-SICM)

We have previously described a current based SICM approach to record the conductance pathways in polymer membranes. Several limitations to these current measurements prevented application to biological samples under physiological conditions. For example, high salt buffers (>1.0 M)[38] and high transmembrane potentials (V_{TM} >500 mV)[39-40] were required to achieve adequate signal-to-noise ratios. To overcome these limitations, we now couple potential based measurements with SICM. In the modified SICM configuration (Figure 1a), a dual-barrel theta pipette is used as the scanning probe (Figure S-1a). One barrel (PE) measures the distance dependent ion current for non-invasive imaging and positioning of the pipette in the same fashion as a normal SICM.[36, 45-49] The second barrel carries an electrode (UE) connected to a differential amplifier and measures potential changes that occur in the vicinity of the pipette tip. Conductive pathways of the sample are measured through changes in the electric field induced by transmembrane potentials applied at the working electrode (WE). To validate measurements made with this approach, potential changes across a polyimide membrane with ~8000 nanopores of 500 nm diameter (Figure S-1b) were recorded. These membranes displayed a transmembrane electrical resistance (TER) of ~94 $\Omega \cdot cm^2$ (in 0.1 M KCl), similar to that of typical epithelial cell monolayers.[50] The potential response (ΔV) was evaluated both in imaging mode (Figure 2b) and in fixed-position mode (Figure 2d). In fixed-position mode, potential deflections were monitored at the pipette (UE) when the pipette was held at a fixed probe-surface distance (D_{ps}) and the WE potential was scanned (Figure 2d). The potential responses at two closely-

NIH-PA Author Manuscript

NIH-PA Author Manuscript

NIH-PA Author Manuscript

spaced nanopores (< 5 μm) over a range of transmembrane potentials are shown (Figure 2a-b). The signal-to-noise ratio from potential measurement was significantly higher (S/N: 17.7) compared to current measurement (S/N: 4.8). To evaluate relative changes in conductance, potential deflections recorded at the pipette tip were measured at a fixed D_{ps} of 0.2 μm, and then referenced to the background response, measured far from the surface (D_{ps} = 12.5 μm). Figure 2d shows the relationship between the applied transmembrane potential (V_{TM}) and the resultant potential deflection (μV) when the pipette is positioned over the center of a membrane pore (pore 1 of Figure 2a in this case). The local conductance (G) over the pore can be estimated from the following equation:[22, 31]

$$G=\left(\frac{E}{\rho \cdot V^{e}}\right)=\left(\frac{\left(\Delta V_{0.2\mu m}-\Delta V_{12.5\mu m}\right)/\Delta z}{\rho \cdot V^{e}}\right)$$

The electric field (E, a potential gradient) is determined by dividing the potential difference ($\Delta V_{0.2\mu m} - \Delta V_{12.5\mu m}$) recorded at two distinct pipette distances (D_{ps}) by the vertical displacement of the pipette (Δz). Here, ρ is the specific resistance of the bath electrolyte and V^{e} is the potential range applied at WE to induce potential deflections (V^{e} = 120 mV in Figure 2d, swept from −60 mV to +60mV). Together, these data indicate that potentiometric SICM (P-SICM) allows ultrasensitive measurements of local conductance at submicron length scales and operating potentials appropriate to probe the physiology of cell-cell junctions.

Differentiation of the paracellular pathway from the transcellular pathway

To perform potential measurements on biological samples, several additional requirements must be fulfilled. First, to prevent disruption of normal physiological function, transepithelial potentials less than 50 mV[22, 51-52] must be used. Second, the application of an alternating transepithelial potential is necessary to avoid polarization of the plasma membrane. Third and most importantly, upon application of an alternating transepithelial potential, the contribution of the reactive components from cell membrane capacitance must be examined. Thus, impedance measurements were performed to determine the appropriate frequency for application of the transepithelial potential. Impedance data recorded at 1 Hz revealed an impedance of 97.3 Ω·cm^2 for wild-type MDCKII (MDCKII-WT) cells (Figure S-2a). This value is in good agreement with ohmic measurements of the TER and indicates error induced by alternating potentials at 1 Hz can be neglected in the P-SICM recording.[22]

For measurements of the apparent paracellular and transcellular conductance, a topographic image of the apical surface of MDCKII cell monolayer was generated with SICM (Figure 3a) in which the locations of the cell junction (CJ) and cell body (CB) were clearly distinguished. High-resolution images afford the ability to position the pipette laterally at the nanometer scale. Recordings were carried out in discrete locations: CJ (for the paracellular pathway) and CB (for the transcellular pathway). To illustrate the relevant size scales, a cell body and a cell junction are indicated in Figure 3a. Here the dimension of the pipette tip is approximated by the diameter of the small black marker inside of the larger white marker. On the time scale of experiments described here, the locations of CJ and CB were stationary. Under an applied transepithelial potential the potential deflection at the pipette was measured by positioning the pipette at either a CJ or a CB. Differences in ΔV recorded at the two D_{ps} (0.2 and 12.5 μm) (Figure 3b) suggested the existence of a heterogeneous potential distribution established by local conductive pathways in the cell monolayer.

Histograms in Figure 4a reflect multiple conductance measurements obtained from three independent experiments on three MDCKII-WT monolayers. Gaussian tests of data revealed

NIH-PA Author Manuscript

NIH-PA Author Manuscript

NIH-PA Author Manuscript

that conductance recorded over CJs and CBs were drawn from normally distributed populations with averages of 6.20 ± 2.54 mS/cm^2 and 2.53 ± 1.49 mS/cm^2, respectively. (Table S-1) Independent two-sample *t*-tests were performed to assess the statistical significance of difference between populations. The resultant *p*-value ($p < 0.001$) indicated that the difference between the paracellular (G^p) and transcellular (G^t) conductances was statistically significant. (Table S-2) Values recorded for G^p and G^t by P-SICM are in good agreement with previously reported measurements of MDCKII cells, which relied upon indirect mathematical deduction to discriminate paracellular and transcellular conductances from the recorded transepithelial conductance.[22, 25] Together, these results highlight the biological significance of P-SICM as a novel tool to measure the relative conductance of paracellular and transcellular channels in polarized epithelia.

P-SICM recording of claudin-2 channel conductance

To demonstrate that P-SICM allows measurement of changes in paracellular conductance, gene expression of claudin-2, a known paracellular channel in MDCKII cells, was knocked down by RNA interference. The knockdown approach to study claudin biology has been established by us previously in several epithelial cell models including MDCKII cells.[14, 18, 53] To confirm the knockdown efficacy for claudin-2 proteins, a monolayer of MDCKII cells which expressed a small interfering RNA (siRNA) against the claudin-2 gene was immunostained (MDCKII-C2; Figure S-2d) and revealed >95% loss of fluorescence signal compared to that in MDCKII-WT cells (Figure S-2c). Impedance measurements revealed a significant increase in the TER of MDCKII-C2 cells (247.95 ± 30.35 Ω·cm^2 versus 113.68 ± 24.98 Ω·cm^2 in MDCKII-WT cells; n=6, $p < 0.001$). Paracellular (G^p) and transcellular (G^t) conductances in MDCKII-C2 cells, shown as histograms in Figure 4b, were recorded by P-SICM. Comparisons of paracellular conductance in MDCKII-C2 versus MDCKII-WT cells (Figure 4c-d) were also measured. The mean paracellular conductance was decreased significantly (57.6%) from 6.20 ± 2.54 mS/cm^2 in MDCKII-WT cells to 2.63 ± 1.26 mS/cm^2 in MDCKII-C2 cells (Figure 4c-d), consistent with the function of claudin-2 as a paracellular channel protein. Notably, there was a small, but significant reduction of the transcellular conductance in MDCKII-C2 cells, which possibly results from interfering changes in surrounding conductive paracellular pathways (see **Discussion**).

P-SICM recording of claudin-2 channel ion selectivity

The most elementary question related to an ion channel is the nature of preferential permeation or rejection of selected ions. An elegant study by Yu et al. found the claudin-2 channel to be aqueous, narrow, and most importantly cation selective.[25] To provide evidence that P-SICM is capable of capturing ion selectivity in paracellular transport, we conducted ion replacement experiments for MDCKII-WT and -C2 cells. For studies of cation selectivity, Na^+ in the basolateral bath solution was substituted with isomolar N-methyl-D-glucamine ($NMDG^+$); for studies of anion selectivity, Cl^- was substituted with gluconate (Glu^-). These organic ions are considered too large to permeate both paracellular and transcellular channels.[5, 7, 54] After $NMDG^+$ or Glu^- replacement, we recorded the conductance for both paracellular (G^p) and transcellular (G^t) pathways and compared to recordings made in Ringer's solution. Conductance differences induced by ion replacement are shown in Figure 5a and 5b for $NMDG^+$ and Glu^-, respectively. $NMDG^+$ substitution significantly decreased the paracellular conductance (33%) in MDCKII-WT cells ($p<0.001$; Table S-3 and S-4), but not in MDCKII-C2 cells (Figure 5a), which indicates claudin-2 is responsible for paracellular cation selectivity. Substitution of Glu^-, barely affected the G^p in MDCKII-WT or -C2 cells (Figure 5b), despite a noticeable trend of G^p reduction of the WT cells. Neither $NMDG^+$ nor Glu^- substitution altered the transcellular conductance of MDCKII-WT or C2 cells, consistent with previous observations that these organic ions cannot permeate the cell membrane.[42] Together, these data demonstrate that P-SICM allows

NIH-PA Author Manuscript

NIH-PA Author Manuscript

NIH-PA Author Manuscript

discrimination of spatially-resolved ion selective conductances through the paracellular channel.

DISCUSSIONS

Recording ion transport of paracellular channels has always been a formidable task. In fact, the existence of paracellular channels in the tight junction has long been debated, due largely to the lack of molecular-level evidence in functioning epithelial tissue. With the improved P-SICM approach, for the first time, conductance at nanometer scales for epithelial tissue is recorded, which allows discrimination of paracellular and transcellular conductances at submicron resolution. The spatial resolution for topographic images reported here is under 100 nm (Figure S-4) and the lateral distribution of potential deflections (ΔV) displays submicron spatial resolution (Figure 2). Resolution in P-SICM measurements is determined largely by the scanning parameters employed, especially the geometry of the pipette tip, the probe-surface distance (D_{ps}) and the potential applied across the sample (V_T). For conditions utilized here, signal measured from pores with nominal radii on the order of 265 nm (Figure S-1b) decayed to three times the background at distances approximately 500 nm from the center of the pore. This distance (500 nm) serves as a good estimate for the lateral resolution of potential measurements. Although our recording approach demonstrated high spatial resolution in a synthetic polyimide membrane (Figure 2), for cell monolayer studies, the continuous distribution of the multitude of competing conductance pathways and the use of a non-zero probe-surface distance (D_{ps}) may result in transcellular artifacts. Manipulation of the continuity of the potential distribution created around a conductive pathway is difficult, so reduction of the probe surface distance (D_{ps}) is a practical way to improve spatial resolution. Additionally, smaller scanning probes can provide a smaller D_{ps} for imaging (in scanning mode) as well as for positioning (in fixed-position mode).[37, 39-40] In addition to improved spatial resolution, smaller probes are also more sensitive in potential measurements because the probe is able to maintain a shorter distance to conductive pathways where variations in local potential are steeper (Figure S-5).

Recorded events of paracellular conductance were far less clustered around the mean value in the histograms of MDCKII-WT (Figure 4a) as compared to MDCKII-C2 cells (Figure 4b). If paracellular conductance in C2 cells represents the background level, then addition of claudin-2 to the tight junction not only increases the mean conductance but also induces variation. Variations in conductance suggest tight junction *dynamics*, such as claudin mobility and claudin-claudin interactions. The claudin channel density along the tight junction strand can be regulated pathophysiologically. For instance, a large number of human mutations found in the claudin-16 gene cause protein trafficking defects.[55-56] Pharmacological chaperones partially rescue these defects and increase the TJ insertion of claudin-16 proteins.[56] The lateral mobility of claudins in the TJ strand, however, is extremely low.[57] Under physiological conditions, there is hardly any exchange of claudin proteins between the tight junction and the intracellular organelles. In fact, over 75% of claudins found in the tight junction are static.[57] These observations rule out the possibility that the variation in paracellular conductance is caused by local thermodynamic mobility of claudin molecules in the tight junction. Claudin proteins are known to interact with each other where TJ strands are formed from *trans* interactions between claudins of adjacent cells, and additional *cis* interactions which assemble as claudin oligomers.[58] These inter and intracellular claudin interactions present in MDCKII cells are likely to result in variations observed in paracellular conductance. Recording errors may also contribute to variation. Although increasing the recording frequency provides a solution, this is difficult in practice because of the large membrane capacitance of the SICM configuration. Beyond application in conductance measurements, SICM presents a valuable tool for the study of local claudin interactions. The highest spatial resolution reported for SICM (3-6 nm)[59] compares

NIH-PA Author Manuscript

NIH-PA Author Manuscript

NIH-PA Author Manuscript

favorably with the resolution of conventional diffraction-limited fluorescence microscopy (FM) (~220 nm), and is comparable to super-resolution FM techniques.[60] In future studies, through selective labeling of claudin species in a culture, SICM promises to locate specific claudin interactions and to measure local claudin function independent of neighboring interactions.

Supplementary Material

Refer to Web version on PubMed Central for supplementary material.

Acknowledgments

Andy Alexander and John Poehlman (Electronic Instrument Services, IU) for instrumentation and Dr. Jim Marr's (IUPUI) for assistance with cell culture are acknowledged. Support of the National Institutes of Health (NIDDK 1R21DK082990), Research Corporation for Scientific Advancement and the American Heart Association to LAB; by the National Institutes of Health Grants R01DK084059 and P30 DK079333, and American Heart Association Grant 0930050N to JH is acknowledged. Alicia Friedman is acknowledged for editorial assistance.

Nonstandard abbreviations

SICM	Scanning ion conductance microscopy
TER	transepithelial resistance
WT	wild type
TJ	tight junction
siRNA	small interference RNA
MDCK	Mardin-Darby Canine Kidney

REFERENCES

1. Van Itallie CM, Anderson JM. Annu. Rev. Physiol. 2006; 68:403–29. [PubMed: 16460278]
2. Tsukita S, Furuse M, Itoh M. Nat. Rev. Mol. Cell Biol. 2001; 2:285–293. [PubMed: 11283726]
3. Reuss, L. Tight junction Permeability to ions and water. In: Cereijido, M.; Anderson, JM., editors. Tight Junctions. 2 ed. CRC Press; New York: 2001. p. 61-88.
4. Farquhar MG, Palade GE. J. Cel. Biol. 1963; 17:375–412.
5. Watson CJ, Rowland M, Warhurst G. Am. J. Physiol. Cell Physiol. 2001; 281:C388–C397. [PubMed: 11443038]
6. Tang VW, Goodenough DA. Biophys. J. 2003; 84:1660–1673. [PubMed: 12609869]
7. Van Itallie CM, Holmes J, Bridges A, Gookin JL, Coccaro MR, Proctor W, Colegio OR, Anderson JM. J. Cell Sci. 2008; 121:298–305. [PubMed: 18198187]
8. Gow A, Southwood CM, Li JS, Pariali M, Riordan GP, Brodie SE, Danias J, Bronstein JM, Kachar B, Lazzarini RA. Cell. 1999; 99:649–59. [PubMed: 10612400]
9. Wilcox ER, Burton QL, Naz S, Riazuddin S, Smith TN, Ploplis B, Belyantseva I, Ben Yosef T, Liburd NA, Morell RJ, Kachar B, Wu DK, Griffith AJ, Friedman TB. Cell. 2001; 104:165–72. [PubMed: 11163249]
10. Furuse M, Hata M, Furuse K, Yoshida Y, Haratake A, Sugitani Y, Noda T, Kubo A, Tsukita S. J. Cell Biol. 2002; 156:1099–111. [PubMed: 11889141]
11. Morita K, Sasaki H, Furuse K, Furuse M, Tsukita S, Miyachi Y. Exp. Dermatol. 2003; 12:289–95. [PubMed: 12823443]
12. Nitta T, Hata M, Gotoh S, Seo Y, Sasaki H, Hashimoto N, Furuse M, Tsukita S. J. Cell Biol. 2003; 161:653–60. [PubMed: 12743111]

NIH-PA Author Manuscript

NIH-PA Author Manuscript

NIH-PA Author Manuscript

13. Kitajiri SI, Furuse M, Morita K, Saishin Kiuchi Y, Kido H, Ito J, Tsukita S. Hear. Res. 2004; 187:25–34. [PubMed: 14698084]
14. Hou J, Shan Q, Wang T, Gomes AS, Yan Q, Paul DL, Bleich M, Goodenough DA. J. Biol. Chem. 2007; 282:17114–17122. [PubMed: 17442678]
15. Simon DB, Lu Y, Choate KA, Velazquez H, Al-Sabban E, Praga M, Casari G, Bettinelli A, Colussi G, Rodriguez Soriano J, McCredie D, Milford D, Sanjad S, Lifton RP. Science. 1999; 285:103–106. [PubMed: 10390358]
16. Van Itallie C, Rahner C, Anderson JM. J. Clin. Invest. 2001; 107:1319–1327. [PubMed: 11375422]
17. Yu ASL, Enck AH, Lencer WI, Schneeberger EE. J. Biol. Chem. 2003; 278:17350–17359. [PubMed: 12615928]
18. Hou J, Gomes AS, Paul DL, Goodenough DA. J. Biol. Chem. 2006; 281:36117–36123. [PubMed: 17018523]
19. Wen H, Watry DD, Marcondes MCG, Fox HS. Mol. Cell. Biol. 2004; 24:8408–8417. [PubMed: 15367662]
20. Hou J, Renigunta A, Konrad M, Gomes AS, Schneeberger EE, Paul DL, Waldegger S, Goodenough DA. J. Clin. Invest. 2008; 118:619–628. [PubMed: 18188451]
21. Frömter E. J. Membr. Biol. 1972; 8:259–301. [PubMed: 5084117]
22. Gitter AH, Bertog M, Schulzke JD, Fromm M. Pfluegers Arch. - Eur. J. Physiol. 1997; 434:830–840. [PubMed: 9306019]
23. Gitter AH, Bendfeldt K, Schulzke JD, Fromm M. Pfluegers Arch. - Eur. J. Physiol. 2000; 439:477–482. [PubMed: 10678745]
24. Florian P, Schoneberg T, Schulzke JD, Fromm M, Gitter AH. J. Physiol. (Lond.). 2002; 545:485–499. [PubMed: 12456828]
25. Yu ASL, Cheng MH, Angelow S, Guenzel D, Kanzawa SA, Schneeberger EE, Fromm M, Coalson RD. J. Gen. Physiol. 2009; 133:111–127. [PubMed: 19114638]
26. Zeissig S, Buergel N, Guenzel D, Richter J, Mankertz J, Wahnschaffe U, Kroesen AJ, Zeitz M, Fromm M, Schulzke JD. Gut. 2007; 56:61–72. [PubMed: 16822808]
27. Heller F, Fromm A, Gitter AH, Mankertz J, Schulzke JD. Mucosal Immunol. 2008; 1:S58–S61. [PubMed: 19079233]
28. Bendfeldt, K.; Gitter, AH.; Fromm, M. Trans- and paracellular conductivity of HT-29/B6 cells measured by high-resolution conductance scanning. In: Wiedenmann, B.; Rosewicz, S.; Zeitz, M.; Riecken, EO., editors. Ann. N.Y. Acad. Sci. Vol. Vol. 859. New York Academy of Sciences; New York, USA: 1998. p. 295-299.
29. Schmitz H, Rokos K, Florian P, Gitter AH, Fromm M, Scholz P, Ullrich R, Zeitz M, Pauli G, Schulzke JD. AIDS. 2002; 16:983–991. [PubMed: 11953464]
30. Gitter AH, Wullstein F, Fromm M, Schulzke JD. Gastroenterology. 2001; 121:1320–1328. [PubMed: 11729111]
31. Cereijido M, Stefani E, Martinezpalomo A. J. Membr. Biol. 1980; 53:19–32. [PubMed: 7373646]
32. Cereijido M, Meza I, Martinezpalomo A. Am. J. Physiol. Cell Physiol. 1981; 240:C96–C102.
33. Cereijido M, Stefani E, Deramirez BC. J. Membr. Biol. 1982; 70:15–25. [PubMed: 7186936]
34. Heller F, Florian P, Bojarski C, Richter J, Christ M, Hillenbrand B, Mankertz J, Gitter AH, Burgel N, Fromm M, Zeitz M, Fuss I, Strober W, Schulzke JD. Gastroenterology. 2005; 129:550–564. [PubMed: 16083712]
35. Gunzel D, Florian P, Richter JF, Troeger H, Schulzke JD, Fromm M, Gitter AH. Am. J. Physiol. Regul. Integr. Comp. Physiol. 2006; 290:R1496–R1507. [PubMed: 16397094]
36. Hansma PK, Drake B, Marti O, Prater CB. Gould SAC. Science. 1989; 243:641–643. [PubMed: 2464851]
37. Chen C-C, Baker LA. Analyst. 2011; 136:90–97. [PubMed: 21103593]
38. Chen C-C, Derylo MA, Baker LA. Anal. Chem. 2009; 81:4742–4751. [PubMed: 19435340]
39. Chen C-C, Zhou Y, Baker LA. ACS Nano. 2011; 5:8404–8411. [PubMed: 21923184]
40. Zhou Y, Chen C-C, Baker LA. Anal. Chem. 2012; 84:3003–3009. [PubMed: 22390616]

NIH-PA Author Manuscript

NIH-PA Author Manuscript

NIH-PA Author Manuscript

41. Amasheh S, Meiri N, Gitter AH, Schoneberg T, Mankertz J, Schulzke JD, Fromm M. J. Cell Sci. 2002; 115:4969–4976. [PubMed: 12432083]
42. Rosenthal R, Milatz S, Krug SM, Oelrich B, Schulzke J-D, Amasheh S, Günzel D, Fromm M. J. Cell Sci. 2010; 123:1913–1921. [PubMed: 20460438]
43. Papini E, Satin B, Norais N, de Bernard M, Telford JL, Rappuoli R, Montecucco C. J. Clin. Invest. 1998; 102:813–820. [PubMed: 9710450]
44. Broughman JR, Brandt RM, Hastings C, Iwamoto T, Tomich JM, Schultz BD. Am. J. Physiol. Cell Physiol. 2004; 286:C1312–C1323. [PubMed: 15151917]
45. Chen C-C, Zhou Y, Baker LA. Annu. Rev. Anal. Chem. 2012; 5
46. Korchev YE, Milovanovic M, Bashford CL, Bennett DC, Sviderskaya EV, Vodyanoy I, Lab MJ. J. Microsc. (Oxf.). 1997; 188:17–23.
47. Novak P, Li C, Shevchuk AI, Stepanyan R, Caldwell M, Hughes S, Smart TG, Gorelik J, Ostanin VP, Lab MJ, Moss GWJ, Frolenkov GI, Klenerman D, Korchev YE. Nat. Methods. 2009; 6:279–281. [PubMed: 19252505]
48. Shevchuk AI, Gorelik J, Harding SE, Lab MJ, Klenerman D, Korchev YE. Biophys. J. 2001; 81:1759–1764. [PubMed: 11509385]
49. Takahashi Y, Murakami Y, Nagamine K, Shiku H, Aoyagi S, Yasukawa T, Kanzaki M, Matsue T. Phys. Chem. Chem. Phys. 2010; 12:10012–10017. [PubMed: 20485766]
50. Gumbiner B, Simons K. J. Cell Biol. 1986; 102:457–68. [PubMed: 3511070]
51. Bindslev N, Tormey JM, Wright EM. Biochim. Biophys. Acta. 1974; 332:286–297.
52. Reuss L, Finn AL. J. Membr. Biol. 1975; 25:115–139. [PubMed: 1214283]
53. Hou J, Renigunta A, Yang J, Waldegger S. Proc. Natl. Acad. Sci. USA. 2010; 107:18010–18015. [PubMed: 20921420]
54. Belloreuss E. J. Physiol. (Lond.). 1982; 326:49–63. [PubMed: 7108807]
55. Hou J, Paul DL, Goodenough DA. J. Cell Sci. 2005; 118:5109–5118. [PubMed: 16234325]
56. Kausalya PJ, Amasheh S, Gunzel D, Wurps H, Muller D, Fromm M, Hunziker W. J Clin Invest. 2006; 116:878–91. [PubMed: 16528408]
57. Shen L, Weber CR, Turner JR. J. Cell Biol. 2008; 181:683–95. [PubMed: 18474622]
58. Furuse M, Sasaki H, Tsukita S. J. Cell Biol. 1999; 147:891–903. [PubMed: 10562289]
59. Shevchuk AI, Frolenkov GI, Sanchez D, James PS, Freedman N, Lab MJ, Jones R, Klenerman D, Korchev YE. Angew. Chem., Int. Ed. 2006; 45:2212–2216.
60. Rust MJ, Bates M, Zhuang X. Nat.Methods. 2006; 3:793–796. [PubMed: 16896339]

NIH-PA Author Manuscript

NIH-PA Author Manuscript

NIH-PA Author Manuscript

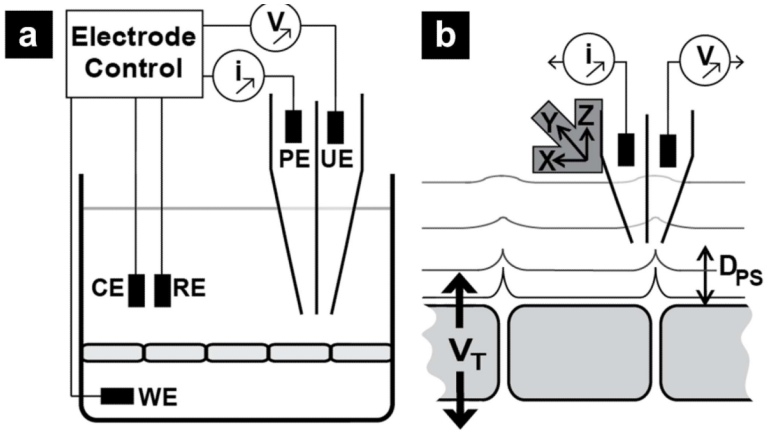

Figure 1.

Illustration of potentiometric scanning ion conductance microscopy (P-SICM) utilized here. (a) A dual-barrel pipette is utilized to measure topographic and potential gradients of a sample of interest. Here the pipette electrode (PE) is used to control pipette position and record topographic images. The potentiometric electrode (UE) records the local potential at the pipette tip. A potential is applied across the sample between the working electrode (WE) and counter electrode (RE). All electrode potentials are referenced to a common reference electrode (RE). (b) Expanded view of the process, the potential applied across the sample (V_T) results in local changes in electric field at conductive pathways within the sample. Position of the dual-barrel probe is achieved with piezo electric positioners that control the probe-surface distance (D_{ps}) and translate the pipette for image collection.

NIH-PA Author Manuscript

NIH-PA Author Manuscript

NIH-PA Author Manuscript

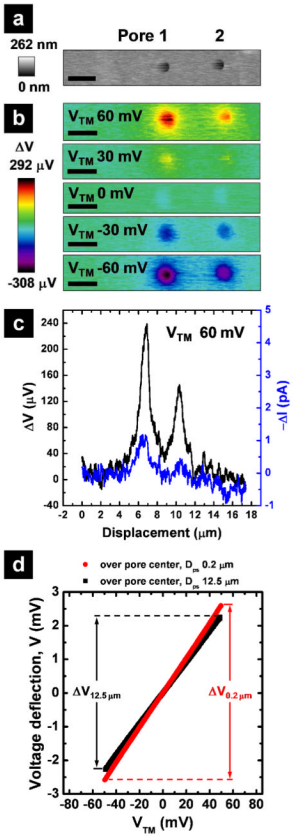

Figure 2.

Characterization of porous membranes with P-SICM. (a) Topography of two pores in a polymer membrane at zero transmembrane potential and (b) images of local potential variations for these two pores at a series of transmembrane potentials (V_{TM}), recorded with P-SICM in imaging mode (Scale bar = 1 μm). Improvement in signal-to-noise ratio gained by potential measurement as compared to current measurement was further exemplified with (c) the line scan across the two pores in question. (d) Changes in the potential deflection at two probe surface distances (D_{ps}), far (12.5 μm) and close (0.2 μm), were recorded in fixed position mode over the center of pore 1. With changes in potential deflection determined at D_{ps} equal to 0.2 μm ($\Delta V_{0.2\,\mu m}$) and D_{ps} equal to 12.5 μm ($\Delta V_{12.5\,\mu m}$), apparent conductance associated with pore 1 can be estimated.

NIH-PA Author Manuscript

NIH-PA Author Manuscript

NIH-PA Author Manuscript

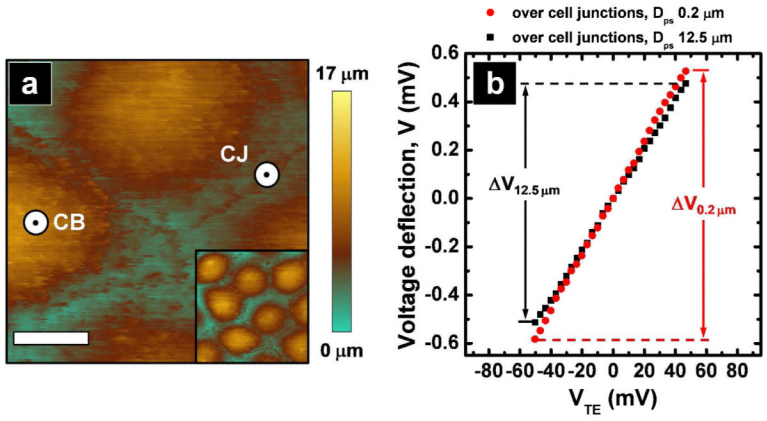

Figure 3.

Characterization of epithelial monolayers with P-SICM (a) Topographic image of the apical surface of a cell monolayer was imaged to locate the position of cell bodies and the cell junctions. Scale bar: 5 μm. The inset shows the zoom out image of the cell monolayer under study (40 × 40 μm). Two positions which illustrate pipette placement are indicated for CB (cell body) and CJ (cell junction). The black marker in the center of the larger white marker at these positions approximates the size of the pipette tip utilized. (b) Potential deflection recorded with fixed position mode at two D_{ps}, far (12.5 μm) and close (0.2 μm), were carried out over the cell junctions to evaluate apparent paracellular conductances.

NIH-PA Author Manuscript

NIH-PA Author Manuscript

NIH-PA Author Manuscript

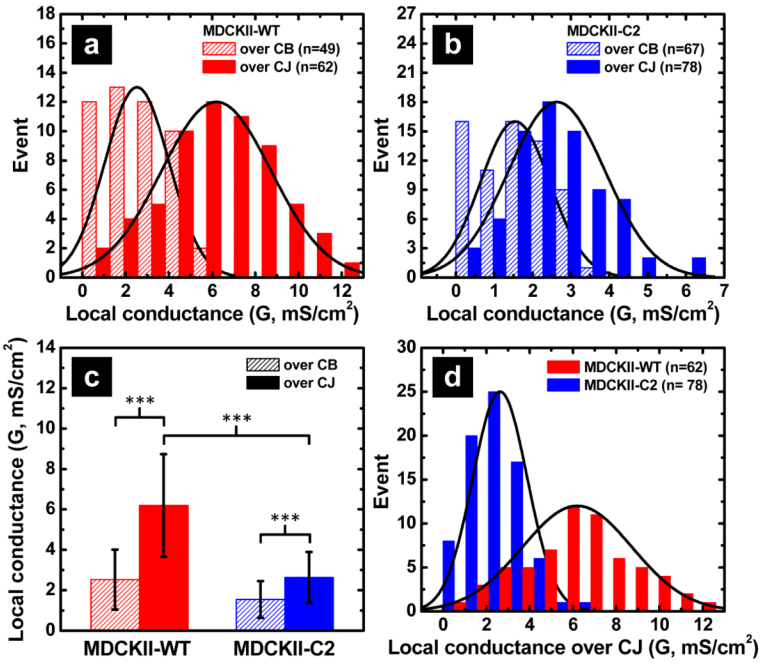

Figure 4.

Apparent conductance measurements recorded with P-SICM (a-b) Histograms of conductance measurements obtained over cell bodies (hatch) and over the cell junctions (solid) on (a) MDCKII-WT and (b) MDCKII-C2 cell monolayers. (c) Average values of local conductance measured for MDCKII-WT (red) and MDCKII-C2 (blue). Statistical significance ($p < 0.001$) between para- and transcellular conductance measured over the cell junction (CJ) and over the cell body (CB) was determined for both MDCKII-WT and MDCKII-C2 monolayers. (d) Histogram of conductances recorded over CJs for MDCKII-WT (red) presents a broader distribution with a larger mean value, as compared to that of MDCKII-C2 (blue). These observations indicate that claudin-2 functions to regulate the epithelial permeability through paracellular pathways.

NIH-PA Author Manuscript

NIH-PA Author Manuscript

NIH-PA Author Manuscript

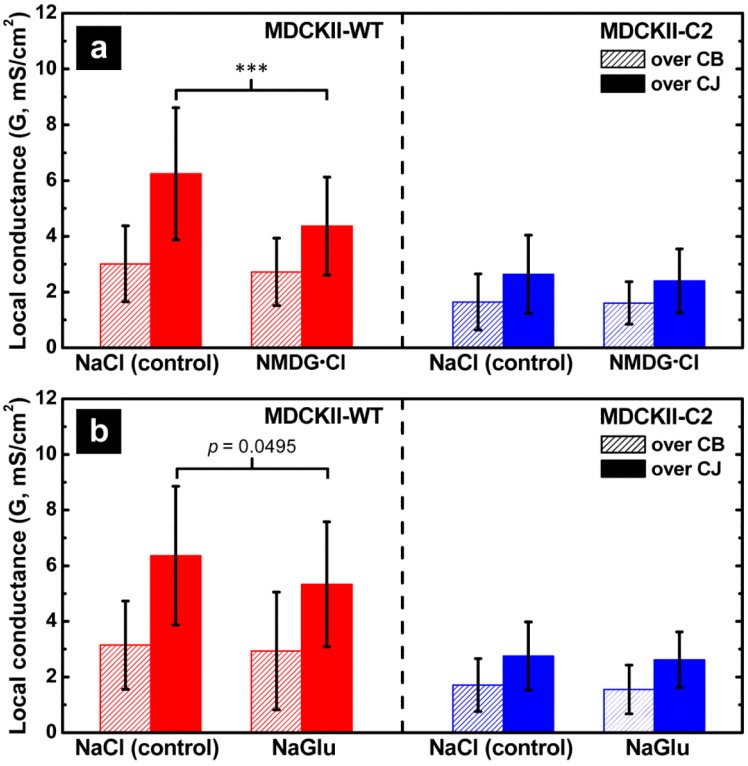

Figure 5.

Ion selectivity of claudin-2 channels investigated with P-SICM. Conductance differences induced by ion replacement with (a) $NMDG^+$ substitution for Na^+ and (b) Glu^- substitution for Cl^- were investigated on both MDCK-WT (red) and MDCKII-C2 (blue) monoalyers. $NMDG^+$ substitution induced significant reduction ($p < 0.001$) in paracellular permeability in MDCKII-WT but not in MDCKII-C2 cells. In contrast, substitution of Glu^- barely affected the paracellular conductance in MDCKII-WT or -C2 cells. Neither $NMDG^+$ nor Glu^- substitution altered the transcellular conductance of MDCKII-WT or C2 cells, consistent with previous observations that these organic ions cannot permeate the cell membrane.